



3D QSAR study, synthesis, and in vitro evaluation of (+)-5-FBVM as potential PET radioligand for the vesicular acetylcholine transporter (VACHT)

Mitja Kovac^a, Sylvie Mavel^{a,*}, Winnie Deuther-Conrad^b, Nathalie Méheux^a, Jana Glöckner^b, Barbara Wenzel^b, Marko Anderluh^c, Peter Brust^b, Denis Guilloteau^a, Patrick Emond^a

^a Université François-Rabelais de Tours, INSERM U930, CHRU, Hôpital Bretonneau, Service de Médecine Nucléaire, 37000 Tours, France

^b Forschungszentrum Dresden-Rossendorf, Research Site Leipzig, Institute of Radiopharmacy, Permoserstr. 15, 04318 Leipzig, Germany

^c University of Ljubljana, Faculty of Pharmacy, Department of Pharmaceutical Chemistry, Aškerčeva 7, 1000 Ljubljana, Slovenia

ARTICLE INFO

Article history:

Received 18 May 2010

Revised 26 May 2010

Accepted 12 August 2010

Available online 17 August 2010

Keywords:

Benzovesamicol derivative

VACHT

Triazene

Fluoro-dediazotiation

3D QSAR

ABSTRACT

Located in presynaptic cholinergic nerve terminals, the vesicular acetylcholine transporter (VACHT) represents a potential target for quantitative visualization of early degeneration of cholinergic neurons in Alzheimer's disease using PET. Benzovesamicol derivatives are proposed as radioligands for this purpose. We report QSAR studies of vesamicol and benzovesamicol derivatives taking into account the stereoselectivity of the VACHT binding site. Use of different data sets and different models in this study revealed that both enantiomers of 5-fluoro-3-(4-phenyl-piperidin-1-yl)-1,2,3,4-tetrahydro-naphthalen-2-ol (5-FBVM) are promising candidates, with predicted VACHT affinities between 6.1 and 0.05 nM. The synthesis of enantiopure (*R,R*)- and (*S,S*)-5-FBVM and their corresponding triazene precursors for future radiofluorination is reported. Both enantiomers exhibited high in vitro affinity for VACHT [(+)-5-FBVM: $K_i = 6.95$ nM and (–)-5-FBVM: $K_i = 3.68$ nM] and were selective for σ_2 receptors (~70-fold), only (+)-5-FBVM is selective for σ_1 receptors (~fivefold). These initial results suggest that (+)-(*S,S*)-5-FBVM warrants further investigation as a potential radioligand for in vivo PET imaging of cholinergic nerve terminals.

© 2010 Elsevier Ltd. All rights reserved.

1. Introduction

The degeneration of cholinergic neurons in the brain is one of the most significant neuropathological features in Alzheimer's disease (AD) synapse disorder has been shown to precede the neurofibrillary and neuritic aspects of AD during the course of the disease,¹ and the loss of synaptic terminals correlates better with cognitive decline than extracellular plaque load or loss of neurons.² Located in presynaptic cholinergic nerve terminals, the vesicular acetylcholine transporter (VACHT) is postulated to be a valuable target for in vivo quantitative visualization of early neurodegenerative processes in AD by using molecular imaging techniques such as SPECT (Single Photon Emission Computed Tomography) and PET (Positron Emission Tomography), PET being regarded as superior in terms of detection efficiency, spatial resolution, and quantification. However, VACHT-specific tracer compounds labeled with the short-lived PET radionuclides ¹⁸F and ¹¹C have not been developed for clinical use to date. Approaches to the development of tracers for VACHT imag-

ing by PET have focused on compounds such as benzovesamicols,^{3–6} trozamicols,^{7,8} or morpholino vesamicols,^{9,10} all based on the structure of (–)-vesamicol, a drug that binds to a side allosteric to the acetylcholine transport side with low-nanomolar affinity.^{11–14} However, (–)-vesamicol possesses moderate affinity to α -adrenoceptors and nanomolar affinity to σ -receptors.¹⁵ In combination with similar expression patterns of VACHT¹⁶ and σ_1 -receptors¹⁷ in the brain the latter cause marginal signal-to-background ratios in in vivo imaging by PET, one reason why so many VACHT radioligands have failed in pre-clinical evaluation to date. On the other hand, the successful application of the benzovesamicol-related SPECT ligand (–)-5-[¹²³I]IBVM (5-iodo-3-(4-phenyl-piperidin-1-yl)-1,2,3,4-tetrahydro-naphthalen-2-ol, $K_d = 0.30$ nM)^{18–21} has encouraged further research into the design of VACHT-specific PET tracers. Structure-affinity studies assessing the potential of iodobenzovesamicol derivatives for visualization of cholinergic terminals have revealed that there is considerable bulk tolerance at different structural positions of the benzovesamicol molecule.^{18,22}

Therefore we have recently synthesized and evaluated new benzovesamicol derivatives²¹ and aza-analogs of trozamicol derivatives both in vitro and in vivo in animals models.^{23–25} Several ¹⁸F-labeled benzovesamicol derivatives have now been synthesized including [¹⁸F]NEFA, [¹⁸F]FAA,⁶ [¹⁸F]FEOBV,⁵ and [¹⁸F]FPOBV³ (Table 1). However, except for [¹⁸F]FEOBV, which is currently

* Corresponding author. Address: Faculté de Pharmacie, Laboratoire de Biophysique Médicale et Pharmaceutique, 31 avenue Monge, 37200 Tours, France. Tel.: +33 2 47 36 72 40; fax: +33 2 47 36 72 24.

E-mail address: sylvie.mavel@univ-tours.fr (S. Mavel).

Table 1
Vesamicol analogs **I** and benzovesamicols **II** used for the QSAR studies



R	I	Ref ^a	R ¹	R ²	R ³	II	Ref ^a
H	(-)-vesamicol (+)-vesamicol	21	H	5-1	H	(-)-5-IBVM (+)-5-IBVM	21
<i>o</i> -CH ₃	(-)- <i>o</i> MV (+)- <i>o</i> MV	30	H	5-N(Et)COCH ₂ F	H	(-)-NEFA	50
<i>p</i> -CH ₃	(-)- <i>p</i> MV (+)- <i>p</i> MV	30	H	5-O(CH ₂) ₂ F	H	(-)-FEOBV (+)-FEOBV	
<i>o</i> -I	(-)- <i>o</i> IV (+)- <i>o</i> IV	52	H	5-(CH ₂) ₃ F	H	(-)-FPOBV (+)-FPOBV	21
<i>m</i> -I	(-)- <i>m</i> IV (+)- <i>m</i> IV	52	H	5-OCH ₂ CHCHI	H	(-)-AOIBV (+)-AOIBV	21
<i>p</i> -I	(-)- <i>p</i> IV	52	H	5-1 and 8-OCH ₃	H	(-)-MOIBV (+)-MOIBV	21
			H	5-1	CH ₂ NH ₂	(-)-MAIBV (+)-MAIBV	21
			H	6-1	H	(-)-6-IBVM	22
			H	7-1	H	(-)-7-IBVM	22
			H	8-1	H	(-)-8-IBVM	22
			<i>p</i> -1	H	H	(-)- <i>p</i> I-BVM	22
			<i>m</i> -1	H	H	(-)- <i>m</i> I-BVM	53
			H	5-NH ₂	H	(-)-ABV (+)-ABV	50
			H	H	H	(-)-BVM	50

^a The data of binding affinities used for QSAR study were taken from these references.

under investigation in PET studies,⁴ these PET tracers have not been suitable for in vivo applications, possibly due to the metabolic susceptibility of the F-carrying substituents, for example, amide in NEFA and alcoholate in FEOBV. In previous paper, FPOBV instability in vivo,³ possibly arising from the weak strength of the C(sp³)-F bond (0.00079 kcal/mol, DiscoveryStudio2.5[®], Accelrys Inc.) causing de-fluorination is reported. To increase the metabolic stability and to reinforce the C-F bond strength by a C(sp²)-F bond (0.0628 kcal/mol, DiscoveryStudio2.5[®], Accelrys Inc.), we have developed the novel benzovesamicol analog 5-FBVM as a fluoro analog of 5-IBVM (Table 1).

In 2008, Szymoszek et al.²⁶ have published a first Comparative Molecular Field Analysis (CoMFA) study using a partial least squares (PLS) algorithm for a set of 37 vesamicol derivatives, covering three different structural types, to predict the binding affinity of vesamicol-type ligands from their respective molecular structure. To expand these efforts, we have performed a further 3D QSAR study, which is based on 32 vesamicol and benzovesamicol derivatives (Table 1) in order to predict the binding affinity for the new compound 5-FBVM. Furthermore, this study considered for the first time the stereoselectivity of the binding of vesamicol derivatives to the VAcHT protein.

Moreover, we also wished to improve the accessibility of the radiolabeling procedure by radiofluorination of non-activated aromatic cycles (i.e., without an electron withdrawing group in *ortho* or *para* position to the leaving group). Therefore, in this report we describe not only the synthesis of 5-FBVM via fluoro-dediazotiation based on the secondary amine 5-ABV, but also the synthesis of a suitable triazene precursor (5-TBV) for future ¹⁸F-labeling. To demonstrate the suitability of triazene as leaving group, the non-radioactive fluorination of 5-TBV resulting in 5-FBVM was accomplished. Because of the stereoselective binding of vesamicol derivatives, 5-ABV was enantioseparated via Mosher ester

synthesis and provided the basis for the synthesis of enantiopure (+)-(S,S) and (-)-(R,R)-5-FBVM as well as (S,S) and (R,R)-5-TBV.

2. Results and discussion

2.1. QSAR study

The QSAR study is based on 32 derivatives which belong to the classes of vesamicols (I) and benzovesamicols (II) (Table 1). Six derivatives were synthesized and evaluated regarding VAcHT affinity and specificity by in-house in vitro assays, the *K_i* values of the remaining compounds were taken from literature. Since binding to the VAcHT is known to be highly enantioselective (generally, the in vitro affinity for the VAcHT of (-)-enantiomers is about 10 times greater) we made three sets from the same overlay: Set 1 for all 32 derivatives, Set 2 for the (-)-enantiomers (20 derivatives), and Set 3 for the (+)-enantiomers (12 derivatives). All the structures were minimized under a CHARMM forcefield with a root mean squared (RMS) difference of energy gradient reached 0.1 kcal/mol Å (Discovery Studio[®] 2.5, Accelrys Inc., San Diego, CA). According to crystallographic findings on vesamicol derivatives^{10,27} and ABV (data not shown, structure see Table 1), the piperidine ring is in a chair conformation, and is almost perpendicular to the cyclohexanol ring, with the hydroxyl in *trans* position as an equatorial conformer. The carbons C-9, C-11, and C-13 of piperidine (see Table 1) and C-OH were chosen for the overlay. *K_i* values were taken from the literature, and p*K_i* = -log *K_i* was used for the Genetic Function Approximation (GFA) algorithm.²⁸ The QSAR program presents 179 physicochemical descriptors as different electronic, spatial, shadow, shape, and thermodynamic indices. After several filters (analyzing the correlation matrix, eliminating the highly correlated descriptors, and eliminating descriptors with too wide a range of training data (>700)), only 26 2D or 3D

descriptors were retained as dependent on pK_i . The definitions of mean descriptors are given in Table 2. In the GFA model, linear or quadratic terms of descriptors were allowed in the selection. For the statistical parameters, the cross validated r^2 is not the most important, and the Friedman's lack-of-fit (LOF) score, which evaluates the QSAR model by considering the number of descriptors as well as the quality of fitness, is chosen: the lower the LOF, the less likely it is that the GFA model will fit the data. The significant regression is given by F , and the higher the value, the better the model. The standard errors of regression coefficients are given in parentheses. GFA models were tested with 5-FBVM, with the excellent predictive sub-nanomolar K_i .

2.1.1. Set 1

$N = 32$: (+) and (–)-enantiomers.

Linear model form: $pK_i(+)(-)\text{pred} = 79.61(\pm 10.49) - 39.86(\pm 5.82) \times JY + 0.99(\pm 0.22) \times \text{Dipole_Z} + 0.0185(\pm 0.004) \times \text{Jurs_PNSA_2} - 4.61(\pm 1.45) \times \text{Shadow_nu} + 3.28(\pm 1.07) \times \text{Bond Energy} - 0.894(\pm 0.348) \times \text{Van der Waals Energy}$.

$r^2 = 0.7425$	$r^2(\text{adj}) = 0.6807$	$r^2(\text{pred}) = 0.6101$	RMS residual error = 0.7419	Friedman L.O.F. = 1.155
----------------	----------------------------	-----------------------------	-----------------------------	-------------------------

Predicted affinity: $pK_i(+)\text{-5-FBVM}_{\text{pred}} = 8.91$ $pK_i(-)\text{-5-FBVM}_{\text{pred}} = 9.34$.

The major contributing factors are $JY > \text{Shadow_nu} > \text{Bond Energy} > \text{Van der Waals Energy} > \text{Dipole_Z} > \text{Jurs_PNSA_2}$.

Quadratic model form: $pK_i(+)(-)\text{pred} = 71.22(\pm 9.53) - 32.92(\pm 4.57) \times JY + 1.03(\pm 0.21) \times \text{Dipole_Z} + 0.0160(\pm 0.003) \times \text{Jurs_PNSA_2} - 4.10(\pm 1.28) \times \text{Shadow_nu} - 0.73(\pm 0.23) \times \text{Bond Energy} \times \text{Van der Waals Energy}$.

$r^2 = 0.7469$	$r^2(\text{adj}) = 0.6982$	$r^2(\text{pred}) = 0.6454$	RMS residual error = 0.7213	Friedman L.O.F. = 1.028
----------------	----------------------------	-----------------------------	-----------------------------	-------------------------

Predicted affinity: $pK_i(+)\text{-5-FBVM}_{\text{pred}} = 9.21$ $pK_i(-)\text{-5-FBVM}_{\text{pred}} = 9.75$.

2.1.2. Set 2

$N = 20$: (–)-enantiomers.

Linear model form: $pK_i(-)\text{pred} = 14.06(\pm 3.67) + 0.0759(\pm 0.0120) \times \text{Molecular_SASA} - 0.0766(\pm 0.011) \times \text{E_ADJ_mag} + 0.9205(\pm 0.0834) \times \text{Jurs_PPSA_3} - 38.88(\pm 7.73) \times \text{Jurs_RPSA} + 2.89(\pm 1.13) \times \text{RadofGyration} - 5.20(\pm 0.76) \times \text{Shadow_nu} - 66.45(\pm 10.20) \times \text{Shadow_XZfrac} + 27.27(\pm 4.31) \times \text{Shadow_YZfrac} - 0.335(\pm 0.051) \times \text{Dihedral Energy}$.

$r^2 = 0.9591$	$r^2(\text{adj}) = 0.9223$	$r^2(\text{pred}) = 0.8523$	RMS residual error = 0.3716	Friedman L.O.F. = 0.6274
----------------	----------------------------	-----------------------------	-----------------------------	--------------------------

Predicted affinity: $pK_i(-)\text{-5-FBVM}_{\text{pred}} = 8.64$.

The major contributing factors are $\text{Shadow_XZfrac} > \text{Jurs_RPSA} > \text{Shadow_YZfrac} > \text{Shadow_nu} > \text{RadofGyration} \approx \text{Jurs_PPSA_3} > \text{Dihedral Energy} > \text{Molecular_SASA} \approx \text{E_ADJ_mag}$.

Quadratic model form: $pK_i(-)\text{pred} = 26.21(\pm 3.37) - 5.32(\pm 0.85) \times JY \times \text{Shadow_nu} - 0.0031(\pm 0.0006) \times \text{Dipole_Z} \times \text{Jurs_PNSA_2} - 0.0053(\pm 0.001) \times \text{Jurs_DPSA_3} \times \text{Dihedral Energy} + 0.145(\pm 0.02) \times \text{Jurs_PPSA_3} \times \text{Shadow_nu}$.

$r^2 = 0.8346$	$r^2(\text{adj}) = 0.7904$	$r^2(\text{pred}) = 0.7359$	RMS residual error = 0.6105	Friedman L.O.F. = 0.7662
----------------	----------------------------	-----------------------------	-----------------------------	--------------------------

Predicted affinity: $pK_i(-)\text{-5-FBVM}_{\text{pred}} = 10.26$.

2.1.3. Set 3

$N = 12$: (+)-enantiomers.

Linear model form: $pK_i(+)\text{pred} = 27.60(\pm 0.02) + 3.42(\pm 0.003) \times \text{CHI_2} - 1.73(\pm 0.001) \times \text{CHI_V_3_P} - 0.059(\pm 0) \times \text{E_ADJ_mag} + 19.66(\pm 0.05) \times \text{JX} - 30.19(\pm 0.05) \times \text{JY} - 0.654(\pm 0.0003) \times \text{Dipole_Z} - 9.64(\pm 0.01) \times \text{Jurs_RPSA} - 3.73(\pm 0.007) \times \text{Shadow_XYfrac} + 3.67(\pm 0.002) \times \text{Bond Energy} - 0.067(\pm 0) \times \text{Dihedral Energy}$.

$r^2 = 1.0000$	$r^2(\text{adj}) = 1.0000$	$r^2(\text{pred}) = 1.0000$	RMS residual error = 0.0004352	Friedman L.O.F. = 1.844e-006
----------------	----------------------------	-----------------------------	--------------------------------	------------------------------

Predicted affinity: $pK_i(+)\text{-5-FBVM}_{\text{pred}} = 8.22$.

The major contributing factors are $JY > JX > \text{Jurs_RPSA} > \text{Shadow_XYfrac} \approx \text{Bond Energy} \approx \text{CHI_2} > \text{CHI_V_3_P} > \text{Dipole_Z} > \text{Dihedral Energy} \approx \text{E_ADJ_mag}$.

The best predictive values for 5-FBVM were obtained with the linear model rather than the quadratic model. Furthermore, considering the (–)-enantioselectivity of VACHT binding site, we focused on (+)/(–) and (–) linear models. For set 1 ((+)/(–) model), the main descriptor was JY (Balaban index which characterizes the shape of a molecule taking into account the relative covalent radius of the atoms of the model) with a mean value for the 32 compounds of 1.50. As the coefficient in the equation was negative, the smaller the value, the better the affinity for the VACHT ($JY_{(-)\text{-5-FBVM}} = 1.460$ compared to $JY_{(-)\text{-IBVM}} = 1.447$ and $JY_{(-)\text{-vesamicol}} = 1.579$). For set 2 ((–) model), the main descriptor was Shadow_XZfrac (a steric descriptor) with a mean value for the 20 compounds of 0.606. The negative coefficient of shadow in the XZ plane indicated that a decrease in the area of the molecular shadow in the XZ plane ($\text{Shadow_XZfrac}_{(-)\text{-5-FBVM}} = 0.577$ compared to $\text{Shadow_XZfrac}_{(-)\text{-IBVM}} = 0.581$ and $\text{Shadow_XZfrac}_{(-)\text{-vesamicol}} = 0.611$) was favorable for affinity for the VACHT. The equations showed multiple occurrence of Jurs descriptors,²⁹ suggesting the importance of charge distribution and surface areas, in particular for the Jurs_RPSA descriptor (total polar surface area divided by the total molecular solvent-accessible surface area) with a mean value for the 20 compounds of 0.0789. Since Jurs_RPSA depends on polar surface, fluorine derivatives had the highest values and the coefficient in the equation was negative. For 5-FBVM the descriptor was the smallest of the fluorine derivatives ($\text{Jurs_RPSA}_{(-)\text{-5-FBVM}} = 0.128$ compared to $\text{Jurs_RPSA}_{(-)\text{-NEFA}} = 0.152$ and $\text{Jurs_RPSA}_{(-)\text{-FEObv}} = 0.130$).

The 3D QSAR model (Discovery Studio[®] 2.5, Accelrys), defines the critical regions (steric or electrostatic) affecting binding affinity. A contour plot of the electrostatic field region favorable (in blue) or unfavorable (red) for the VACHT affinity is shown in Figure 1 with the superposition of both stereoisomers. As reported by the 3D QSAR modeling shown that substitutions near the 5-position should increase the affinity for VACHT (as it was previously suggested by Szymoszek et al.²⁶) as well as an electropositive substituent (near the 8-position) as shown in Figure 2. A good ligand should have strong Van der Waals attraction in the green area and a polar group in the blue electrostatic potential area. Figure 3 shows the differences obtained for the 3D QSAR model with positive coefficients (in green) on a Van der Waals grid between the (–)-enantiomers model and the (+)-enantiomers model. Moreover we observed an overlap of a negative yellow area near the 5-position for (+)-enantiomer FBVM in the favorable positive green area of (–)-enantiomers model, this could explain partially the stereospecificity of VACHT binding site. With this good 3D model ($N = 32$) $pK_i(-)\text{-5-FBVM} = 9.72$ and $pK_i(+)\text{-5-FBVM} = 8.24$ with $r = 0.922$ and $r^2 = 0.851$ could be predicted, corresponding to the experimental finding reported in Table 3 ($pK_i = 8.43$ and 8.16, respectively).

A third QSAR study was performed based on Bayesian modeling (Discovery Studio[®] 2.5, Accelrys) which distinguishes 'active'

Table 2
Description of the molecular properties used as descriptors in QSAR studies

Property	Description	Description
Molecular_SASA	2D surface area	Total solvent accessible surface area
CHI-2	2D topological descriptors	Unmodified molecular connectivity indices. This type of emphasizes different aspects of atom connectivity within a molecule—the amount of branching, ring, structures present and flexibility
CHI-V_3_P	2D topological descriptors	
E_ADJ_mag	2D topological descriptors	
JX	2D topological descriptors	Highly discriminating descriptor. This Balaban indices characterize the shape of a molecule taking into account electronegativity of the atoms of the model
JY	2D topological descriptors	Highly discriminating descriptor. This Balaban indices characterize the shape of a molecule taking into account relative covalent radius of the atoms of the model
Shadow XZ frac	Spatial	Projection of molecular surface on a plan (XZ)
Shadow XY frac	Spatial	Projection of molecular surface on a plan (XY)
Shadow YZ frac	Spatial	Projection of molecular surface on a plan (YZ)
Shadow_nu	Spatial	Ratio of largest to smallest dimension of projection of molecular surface on a plan
Dipole Z	3D electronic descriptors	Dipole moment
Jurs_PNSA_2		Total charge weighted negative surface area
Jurs_PPSA_3		Atomic charge weighted positive surface area
Jurs_RPSA		Relative polar surface area: total polar surface area divided by the total molecular solvent-accessible surface area
RadofGyration	3D molecular properties	
Angle energy	Molecular properties	Conformational
Bond energy	Molecular properties	Conformational
Electrostatic energy	Molecular properties	
Dihedral energy	Molecular properties	
Van der Waals energy	Molecular properties	Conformational

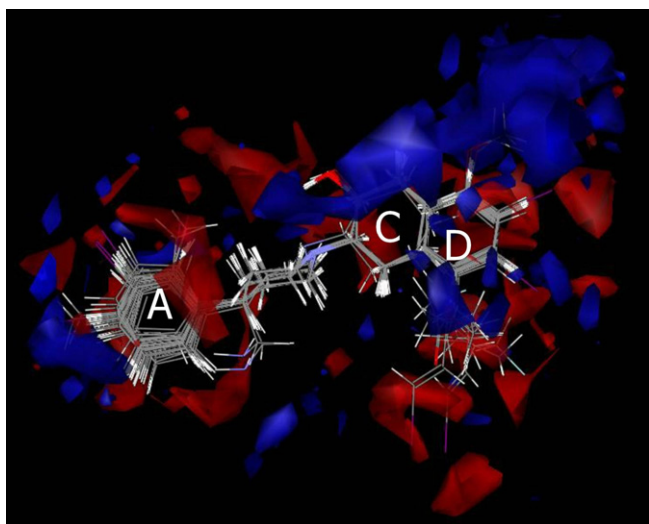


Figure 1. Isosurface of the 3D QSAR model coefficients on Electrostatic Potential grids with positive (in blue) and negative (in red) coefficients for the aligned molecular structures of 32 (+)/(–)-enantiomers I and II in solid representation (A, C, and D visualize cycles as precise in Table 1).

ligands from baseline ligands. The Bayesian statistics assign the probability for each individual descriptor of a molecule to be a member of an 'active' class. From the data set of 32 known ligands (Table 1), 81% were defined as 'active' or 'inactive', with a cutoff value at a $pK_i = 7.69$ ($K_i < 25$ nM). From this effective model we tested (–) and (+)-5-FBVM to predict their activity. The results did not

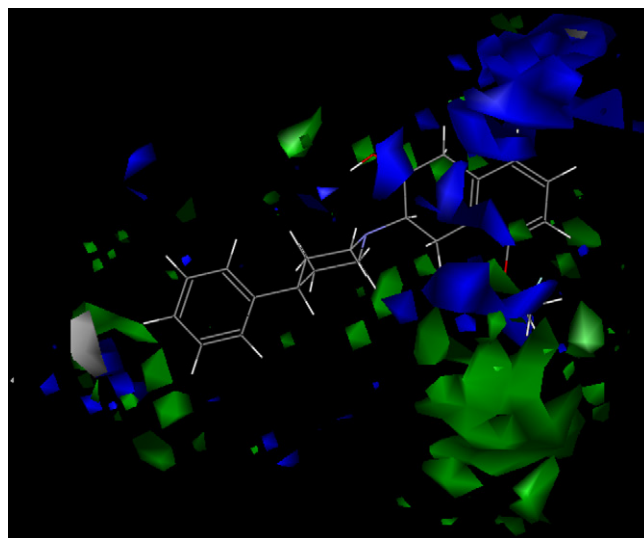


Figure 2. Isosurface of the 3D QSAR model positive coefficients on Van der Waals grid (in green) and Electrostatic Potential grid (in blue) for (+)/(–)-enantiomer model in solid representation with (–)-5-FE0BV.

distinguish these two enantiomers, they were both predicted as 'active' with a probability of 82%. From the listing scores obtained in this Bayesian model, the closest compound of FBVM was (–)-oMV, which presented a $K_i = 6.7$ nM,³⁰ that is, was close to the experimental findings ($K_{i(-)-5-FBVM} = 3.7$ nM and $K_{i(+)-5-FBVM} = 6.9$ nM, Table 3).

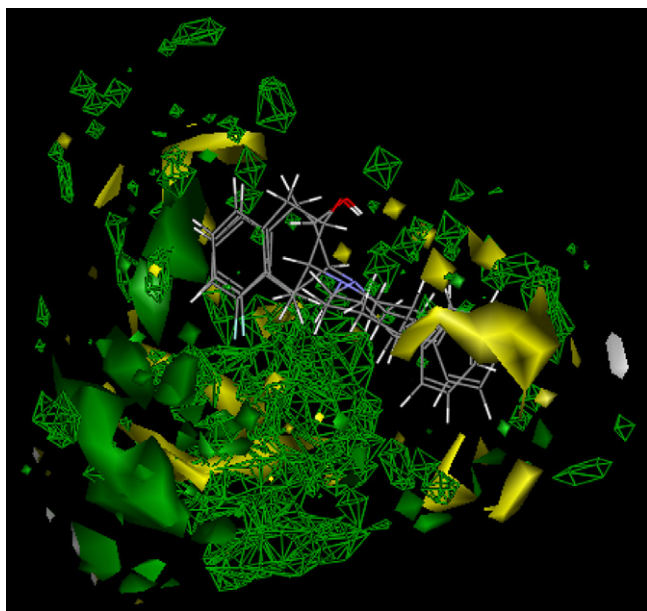
Table 3Affinities and selectivity of FEOBV, (rac)-5-IBVM, (rac)-5-ABV, and 5-FBVM for rVAcHT, σ_1 and σ_2 (K_i values are given in means \pm SD)

	rVAcHT	K_i values, in nM		Ratio of K_i values	
		σ_1	σ_2	σ_1 /VAcHT	σ_2 /VAcHT
(-)-FEOBV	19.6 \pm 1.1 ^a	209 \pm 94 ^a	n.d.	10.7	n.c.
(+)-FEOBV	56.9 \pm 4.8 ^a	269 \pm 37 ^a	n.d.	4.7	n.c.
(rac)-5-IBVM	15.8 \pm 5.42	266 \pm 113 ^a	n.d.	17	n.c.
(rac)-5-ABV	40.6 \pm 1.69	652 \pm 60	n.d.	16	n.c.
(rac)-5-FBVM	10.9 \pm 2.78	13.2 \pm 5.84	229 \pm 60 ^a	1.21	21
(+)-(S,S)-5-FBVM	6.95 \pm 0.62 (p <i>K</i> _i = 8.16)	38.1 \pm 4.85	526 ^b	5.48	76
(-)-(R,R)-5-FBVM	3.68 \pm 0.48 (p <i>K</i> _i = 8.43)	3.57 \pm 0.86	252 \pm 13 ^a	0.97	68

 K_i values were determined by competition of derivatives against bound (-)-[³H]vesamicol under equilibrium at 22 °C, unless stated.

n.d.: not determined.

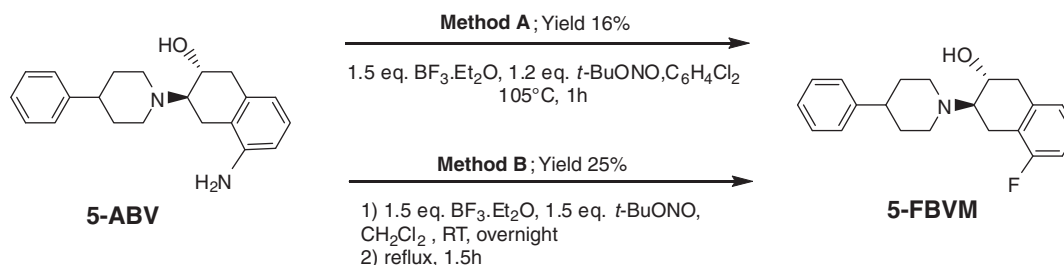
n.c.: not calculated.

All experiments were performed in triplicate ($n \geq 3$; ^a $n = 2$; ^b $n = 1$).**Figure 3.** Isosurface of the 3D QSAR model positive coefficients on Van der Waals grids in green and negative coefficients on Van der Waals grid in yellow: in solid representation for (+)-enantiomers model, in quad mesh representation for (-)-enantiomers model with (+) and (-)-5-FBVM.

From these three QSAR studies, 5-FBVM is predicted to be a ligand with nanomolar VAcHT binding affinity, without significant differences between the two enantiomers.

2.2. Chemistry

Synthesis of the 5-ABV enantiomers which were the basis for all fluorinations has already been described.^{5,27,31}

**Scheme 1.** Synthesis of 5-FBVM from 5-ABV by one pot fluoro-dediazotization.

The Balz-Schiemann reaction (1927) is a well known process of deamine fluorination of aniline via the $\text{S}_{\text{N}}1$ mechanism by the action of sodium nitrite (NaNO_2), followed by thermal decomposition with fluoroboric acid (HBF_4). The mechanism of halogeno-dediazotization may take place via an ionic pathway (heterolytic decomposition)^{32,33} or via a radical pathway.³⁴ An alkyl nitrite such as *n*-butylnitrite or *t*-butylnitrile, that is, soluble in organic solvents could be a good diazotizing agent according to the literature.^{35,36} Moreover they are very weak electrophiles (even weaker than the nitronium ion). The solvent, which is one of the key parameters for a successful reaction, should be a chlorinated organic solvent because it is aprotic and presents non-nucleophilic and non-oxidizing properties. Ionic liquid solvents are known to improve the yield of the Balz-Schiemann reaction.^{37,38} Because of the high redox potential of fluoride anion (e.g., F_2/F^- in CH_3CN $E = 2.4$ V), the formation of a fluoroaryl bond proceeds generally via a heterolytic mechanism.³⁹ Furthermore, the redox potential could be increased by solvation.³⁹ The source of the fluorine atom is variable: silicium fluoride (SiF_4) is fairly toxic; alkali metal fluorides (CsF or KF) are hygroscopic with poor solubility; and quaternary ammonium fluorides are very hygroscopic but are soluble in aprotic solvents. Other salts such as boron trifluoride-diethyl etherate ($\text{BF}_3 \cdot \text{Et}_2\text{O}$) are excellent fluorinating agents³⁵ and are soluble in chlorinated solvents in contrast to nitronium tetrafluoroborate (NOBF_4) or nitronium hexafluorophosphate (NOPF_6). The decomposition temperature of the diazonium group depends on further substituents on the aromatic ring.⁴⁰

We tested several fluorinating agents and reaction conditions such as (i) 1.5 equiv of NOBF_4 , CH_2Cl_2 , 1 h reflux; (ii) 1.5 equiv of NaBF_4 , 1.5 equiv $t\text{-BuONO}$, CH_2Cl_2 , 1 h, rt; (iii) 1.5 equiv of $(t\text{-Bu})_4\text{NF}$, 1.5 equiv $t\text{-BuONO}$, CH_2Cl_2 , 1 h, reflux; and (iv) 1.5 equiv of $\text{BF}_3 \cdot \text{Et}_2\text{O}$, 1.2 equiv $t\text{-BuONO}$, $\text{C}_6\text{H}_4\text{Cl}_2$, 1 h, 60 °C. **Scheme 1** presents the best results of one pot fluoro-dediazotiation of the primary aromatic amine 5-ABV to obtained 5-FBVM in moderate yield (around 25% yield). The chlorinated organic solvents dichlorobenzene (method A)³⁵ or CH_2Cl_2 (method B) were suitable for such

one pot fluoro-dediazoniation. Increasing of the amount of nitrite or fluorine agent (2 equiv) did not increase the yield (12% yield).

Since this method is not useable for radiolabeling, we developed a further procedure to introduce a fluorine atom, in particular for future ^{18}F -radiofluorination. Aryl-dialkyltriazenes (as a protected form of aryldiazonium ions) have been extensively studied for different purposes (for review, see Ref. 41). We synthesized triazene 5-TBV precursors using two methods: the typical method via a diazonium salt quenched with diethylamine to provide 5-TBV in quantitative yield (method A, Scheme 2), and method B started by the synthesis of a diazonium salt obtained by using *t*-butylnitrite in CH_2Cl_2 then quenched with diethylamine to provide 88% yield of 5-TBV. Triazenes can be decomposed by acidic-thermal-decomposition through diazonium ion to provide fluorinated^{42,43} or iodinated⁴⁴ derivatives as described for certain radiolabelings. Two pathways are possible: photoinduced decomposition of 1-aryl-3,3-dialkyltriazenes or thermal decomposition via ionic paths.³⁹ Both processes start with cleavage of the N(2)–N(3) bond.³⁴ Most studies agree on strong acid-catalyzed decomposition of triazenes, involving fast and reversible protonation of N(3), followed by the ‘slow’ heterolytic cleavage of the N(2)–N(3) bond to yield the corresponding diazonium ion and amine.^{39,45–47} Protonation of N(3) is a crucial step to decompose the triazeno moiety (competing with N(1) protonation): the partial atom charges of N(1) and N(3) for 5-TBV were -0.138 and -0.0912 , respectively (Discovery Studio[®] 2.5, CFF forcefield, Accelrys Inc), corresponding to the dipolar charge distribution of the triazene functional group.

Because the triazene moiety is decomposed through a diazonium ion, the theoretical model for acid-catalyzed thermal decomposition to yield the desired arylfluoride (fluoro-de-triazenation) is the same as for fluoro-dediazoniation.⁴⁸ This acid should not present a nucleophilic conjugated base (A^-) to prevent competition with fluoride anion for aryl cation. Additionally, an acid with a low redox potential (e.g., trifluoroacetic acid) is desirable, to prevent reduction of the aryldiazonium ion via the radical pathway and the formation of radicals.

For the synthesis of (\pm)-5-FBVM from the aryl-dialkyltriazenes (\pm)-5-TBV we first tested TBFA in $\text{C}_6\text{H}_4\text{Cl}_2$ or in CH_2Cl_2 at reflux and *p*-toluenesulfonic acid (PTSA) with a high redox potential

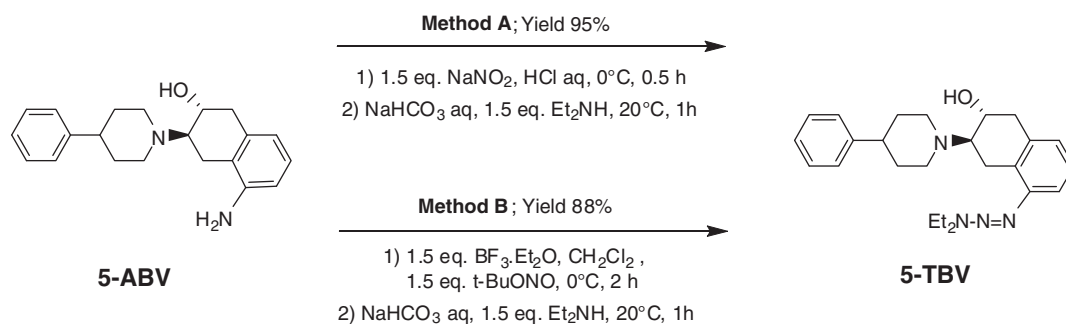
and non-nucleophilic properties. However, we observed the formation of the corresponding aryl-*p*-toluenesulfonic ester analog. In contrast, the reaction with triflic acid in CH_2Cl_2 was more successful, and we obtained 5-FBVM with 25% yield (Scheme 3). A chlorinated organic solvent, especially CH_2Cl_2 (compared to $\text{C}_6\text{H}_4\text{Cl}_2$), was a good solvent, possibly due to the potential stabilization of the diazonium-boron trifluoride complex intermediate. We also tested several fluorinating agents, including tetra-*n*-butylammonium fluoride (TBAF), which is soluble in chlorinated solvents. Reaction of TBAF, CH_2Cl_2 , and $\text{CF}_3\text{SO}_3\text{H}$ under reflux was not successful (data not shown). The use of CsF in carbon tetrachloride with triflic acid, as previously described for dimethyltriazenes,⁴⁹ failed in our case (data not shown), possibly due to the insolubility of CsF and triflic acid in CCl_4 . Using KF in $\text{C}_2\text{H}_4\text{Cl}_2$ at reflux was also not successful.

The enantiomeric purity and the optical rotation of (*S,S*)- and (*R,R*)-5-FBVM were checked by chiral HPLC by using an amylose based column in RP mode (91% $\text{CH}_3\text{CN}/20\text{ mM NH}_4\text{OAc aq}$) and a chiral detector. Under these conditions, (*S,S*)-5-FBVM was a (+)-enantiomer and (*R,R*)-5-FBVM a (–)-enantiomer.

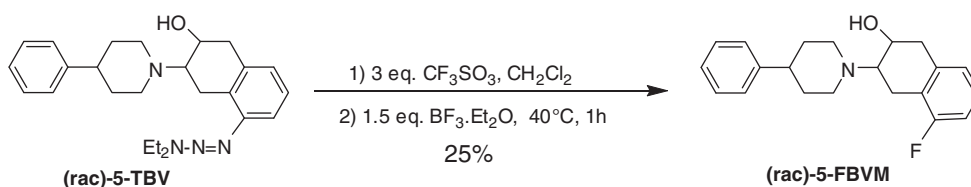
2.3. In vitro evaluation

Vesamicol-derived ligands are generally insufficiently selective towards VACHT due to a non-negligible affinity to σ receptors. Since these receptors are distributed in cholinergic brain areas, specific imaging of cholinergic deficiency is almost impossible with unselective compounds.

Binding affinities of 5-FBVM and reference compounds to VACHT and σ receptor sites were determined in vitro with K_i values presented in Table 3. 5-FBVM presents very good affinity for VACHT and, surprisingly, the (+)-(*S,S*) enantiomer showed almost the same affinity as the (–)-(*R,R*) enantiomer ($K_{i(S,S)FBVM} = 6.95\text{ nM}$ and $K_{i(R,R)FBVM} = 3.68\text{ nM}$), the affinity being better than for ABV ($K_i = 6.95\text{ nM}$), that is, known to be a good ligand.⁵⁰ Furthermore, (+)-(*S,S*)-5-FBVM is selective for VACHT towards the σ_1 receptor ($K_{i(S,S)} = 38.1\text{ nM}$ and $K_{i(R,R)} = 3.75\text{ nM}$), and both isomers are selective for VACHT towards σ_2 receptors ($K_i > 200\text{ nM}$). The affinity of 5-FBVM is in the same range as the affinity of 5-IBVM which is currently regarded as the standard radiotracer.



Scheme 2. Synthesis of (*S,S*) and (*R,R*)-5-TBV.



Scheme 3. Synthesis of (*rac*)-5-FBVM from triazene precursor (*rac*)-5-TBV.

3. Conclusion

We obtained a good linear GFA model and a 3D QSAR model which confirmed the spatial impact on affinity for VACHT via steric descriptors and the Van der Waals coefficient. Each study predicted a good affinity of both 5-FBVM enantiomers.

All one pot acid-catalyzed thermal fluoro-dediazotiation reactions confirmed that parameters such as good solubility, non-nucleophilicity, and high redox potential of the reagents used, such as triflic acid, are the most important conditions for successful fluoro-detriazination via the formation of diazonium ion. Using boron trifluoride etherate we succeeded in introducing fluorine on an aromatic nucleus. Dichloromethane proved to be the most opportune solvent for one pot fluoro-dediazotiation. The in vitro evaluations confirmed the QSAR model where both enantiomers exhibited high affinity for VACHT [(+)-5-FBVM: $K_i = 6.95$ nM and (–)-5-FBVM: $K_i = 3.68$ nM]. The stereoisomers were selective towards σ_2 receptors (~70-fold), however, only (+)-5-FBVM is also selective for σ_1 receptors (~fivefold). Further experiments are needed to improve the characterization of the pharmacological and pharmacokinetics profiles of this compound in order to determine its potential use as an F-18-labeled imaging agent for studies involving the cholinergic system.

4. Experimental section

4.1. Molecular modeling

Computational results were obtained using software programs from Accelrys Software Inc. The molecules were built and minimized in molecular package (Discovery Studio[®] 2.5.5, Accelrys, San Diego, CA) by CHARMM with CFF partial charge estimation method. The GFA model in QSAR protocol was used with a population size of 100 and 5000 maximum generations. All the parameters have been left to the system defaults. Two model forms have been used: linear or full quadratic. For the 3D QSAR model, the grid spacing was 1 Å.

4.2. Chemistry

NMR spectra were recorded on a Bruker DPX Avance 200 spectrometer (200 MHz for ¹H, 50.3 MHz for ¹³C). CDCl₃ was used as solvent; chemical shifts are expressed in ppm relative to TMS as an internal standard. Mass spectra were obtained on a CG-MS Hewlett Packard 5989A spectrometer (electronic impact at 70 eV). The thin-layer chromatographic (TLC) analyzes were performed using Merck 60-F₂₅₄ silica gel plates. Flash chromatography was used for routine purification of reaction products using silica gel (230–400 mesh). Visualization was accomplished under UV or in an iodine chamber. All chemicals and solvents were of commercial quality and were purified following standard procedures. Elemental analyzes of new compounds were within ±0.5% of theoretical values.

4-Phenylpiperidine, used in the synthesis of 5- and 8-amino-benzovesamicol (ABV),²⁷ was obtained by alkaline fusion from 4-cyano-4-phenylpiperidine.³¹ Enantiomeric resolution of 5-ABV was done by chromatography separation of diastereomeric *N,O*-bis-(–)- α -methoxy- α -trifluoromethylphenylacetyl (MTPA) derivatives followed by hydrolysis of Mosher esters.⁵ The optical purity of both (–)-ABV and (+)-ABV was checked on Chiracel OD column (4.6 × 250 nm, 10 μ m particle, Daicel Chemical Industries Ltd, Illkirch France) with *n*-hexane/isopropanol (80/20) as eluent at a flow rate of 1.5 mL/min ((+)-ABV; $t_R = 11$ min, (–)-ABV; $t_R = 13.5$ min).

(–)-5-IBVM^{18,27} and (–)-FEOBV⁵ were synthesized as previously described.

4.2.15-Fluoro-3-(4-phenyl-piperidin-1-yl)-1,2,3,4-tetrahydronaphthalen-2-ol: 5-FBVM from 5-ABV

4.2.1.1 Method A.

To a cold (0 °C) solution of (rac)-5-ABV (0.161 mg, 0.5 mmol) in anhydrous 1,2-dichlorobenzene (4 mL), boron trifluoride diethyl etherate (BF₃·O(CH₂CH₃)₂) (0.064 mL, 0.75 mmol) was added. The stirred reaction mixture was warmed to 105 °C and *n*-butylnitrite (0.07 mL, 0.6 mmol) was added. The mixture was warmed for 1 h. After cooling to room temperature, the solution was quenched with water and extracted with EtOAc. The water phase was made basic by Na₂CO₃ and was extracted once again with EtOAc. The combined organic extracts were dried over MgSO₄ and concentrated under reduced pressure. The crude product was purified by gradient flash chromatography (Al₂O₃, *n*-hexane/EtOAc 4/1 to *n*-hexane/EtOAc 1/1). (rac)-5-FBVM was obtained as a white powder in 16% yield.

4.2.1.2. Method B.

To a cold (0 °C) solution of (rac)-5-ABV (0.161 mg, 0.5 mmol) in anhydrous dichloromethane (4 mL) boron trifluoride diethyl etherate (BF₃·O(CH₂CH₃)₂) (0.064 mL, 0.75 mmol) and *n*-butylnitrite (0.095 mL, 0.75 mmol) were added. The mixture was stirred at room temperature overnight and afterward heated to 60 °C for drying. After cooling, water was added to this reaction residue. The water phase was made basic by NaHCO₃ and was extracted with EtOAc for two times. The combined organic extracts were dried over MgSO₄ and concentrated under reduced pressure. The crude product was purified by gradient flash chromatography (SiO₂, *n*-hexane/EtOAc 4/1 to *n*-hexane/EtOAc 1/2). (rac)-5-FBVM was obtained as a white powder in 25% yield.

(+)-5-FBVM and (–)-5-FBVM were obtained by the same procedure as white powders in 27% and 25% yield, respectively, starting from the corresponding (+)-5-ABV and (–)-5-ABV.

¹H NMR (CDCl₃): δ 1.75–1.96 (m, 4H, 4H-10), 2.53–3.08 (m, 9H, 1H-11, 1H-1, 2H-4, 1H-3, 4H-9), 3.25 (dd, $J = 5.4$ Hz, $J = 16$ Hz, 1H-1), 3.85–3.99 (m, 1H-2), 4.34 (br s, OH), 6.86–6.97 (m, 1H_{Ar}), 7.10–7.17 (m, 2H_{Ar}), 7.26–7.41 (m, 5H_{Ar}).

¹³C NMR (CDCl₃): δ 19.0 (C-4), 33.7, 34.2 (2C-10), 37.6 (C-1), 42.8 (C-11), 44.8, 53.4 (2C-9), 65.1 (C-2), 65.9 (C-3), 112.1 (² $J_{C-F} = 22$ Hz, C-6), 122.5 (² $J_{C-F} = 18$ Hz, C-4a), 124.5 (⁴ $J_{C-F} = 3$ Hz, C-8), 126.2 (CH_{Ar}), 126.7 (2CH_{Ar}), 127.1 (³ $J_{C-F} = 8$ Hz, C-7), 128.4 (2CH_{Ar}), 136.5 (³ $J_{C-F} = 8$ Hz, C-8a), 145.9 (C_{Ar}), 160.9 (¹ $J_{C-F} = 243$ Hz, C-5).

MS: $m/z = 325$ (14), 228 (74), 174 (35), 161 (18), 155 (16), 146 (100), 133 (32), 56 (31).

Anal. Calcd for rac-C₂₁H₂₄FNO: C, 77.51; H, 7.43. Found: C, 77.90; H, 3.91.

4.2.25-(3,3-Diethyltriaz-1-enyl)-3-(4-phenylpiperidin-1-yl)-1,2,3,4-tetrahydronaphthalen-2-ol: (rac)-5-ABV-diethyltriazene (5-TBV)

4.2.2.1 Method A.

(rac)-5-ABV (256 mg, 0.8 mmol) was dissolved in 0.1 mL of 12 N HCl and the flask was immersed in an ice-bath (0–5 °C). A 1.5 equiv of NaNO₂ (82 mg) was added to the solution and the reaction mixture was stirred for 30 min. After neutralization with saturated aqueous solution of NaHCO₃, 1.5 equiv of diethyl amine (0.12 mL) was added to react for 1 h. The mixture was extracted three times with CH₂Cl₂. Combined organic extracts were dried over MgSO₄ and concentrated under reduced pressure. The triazene (rac)-5-TBV was obtained as a white powder and was pure enough to be used without any purification (95% yield).

(+)-5-TBV and (–)-5-TBV were obtained by the same procedure as white powders in 92% or 96% yield, respectively, starting from the corresponding (+)-5-ABV and (–)-5-ABV.

4.2.2.2. Method B.

(rac)-5-ABV (256 mg, 0.8 mmol) was dissolved in CH₂Cl₂ (2 mL) and the flask was immersed in an ice-bath

(0–5 °C). A 1.5 equiv of boron trifluoride diethyl etherate (0.15 mL) and 1.5 equiv of *t*-butylnitrite (0.14 mL) were added to the stirred solution. After 2 h, the reaction mixture was neutralized with saturated aqueous solution of NaHCO₃ and 1.5 equiv of diethyl amine (0.12 mL) was added and stirred for 1 h. The mixture was quenched with water and extracted three times with CH₂Cl₂. Combined organic extracts were dried over MgSO₄ and concentrated under reduced pressure. The triazene (rac)-5-TBV was pure enough to be used without any purification (88% yield).

¹H NMR (CDCl₃): δ 1.34 (t, *J* = 7 Hz, 6H, 2CH₃), 1.76–2.01 (m, 4H, 2H-10, 2H-12), 2.48–3.08 (m, 8H, 1H-11, H-1, 2H-4, 2H-9, 2H-13), 3.37 (dd, *J* = 5.6 Hz, *J* = 16 Hz, 1H-1), 3.45 (dd, *J* = 3.4 Hz, *J* = 15.5 Hz, 1H-1), 3.83 (q, *J* = 7 Hz, 4H, 2CH₂), 3.91–3.97 (m, 1H-2), 6.95 (d, *J* = 6.5 Hz, 1H_{Ar}), 7.15–7.37 (m, 7H_{Ar}).

¹³C NMR (CDCl₃): δ 12.6 (br s, 2CH₃); 21.5 (C-4), 33.8, 34.3 (2C-10), 38.1 (C-1), 42.8 (C-11), 45.0, 53.5 (2C-9), 65.4 (C-2), 66.7 (C-3), 114.0 (CH_{Ar}), 125.9, 126.1, 126.3 (3CH_{Ar}), 126.7 (2CH_{Ar}), 128.4 (2CH_{Ar}), 129.4 (C_{Ar}), 134.6 (C_{Ar}), 146.1 (C_{Ar}), 148.9 (C_{Ar}).

MS: *m/z* = 307 (84), 174 (100), 129 (26), 117 (44), 115 (41), 91 (49), 70 (33).

4.2.3. (rac)-5-Fluoro-3-(4-phenyl-piperidin-1-yl)-1,2,3,4-tetrahydro-naphthalen-2-ol: (rac)-5-FBVM from 5-triazene 5-TBV

To a solution of (rac)-5-TBV (0.162 g, 0.4 mmol) in anhydrous CH₂Cl₂ (5 mL) trifluoromethanesulfonic acid monohydrate (CF₃SO₃H·H₂O) (0.18 mg, 1.2 mmol) dissolved in CH₃CN (0.5 mL) was added. BF₃·Et₂O (boron trifluoride diethyl etherate, 0.075 mL, 0.6 mmol) diluted in CH₂Cl₂ (0.2 mL) was then added to the stirred reaction mixture. The reaction mixture was heated to 60 °C for drying over 1 h. After cooling, water was added to this reaction residue. The water phase was made basic by NaHCO₃ and was extracted with CH₂Cl₂. The combined organic extracts were dried over MgSO₄ and concentrated under reduced pressure. The crude product was purified by gradient flash chromatography (SiO₂, *n*-hexane/EtOAc 4/1 to *n*-hexane/EtOAc 1/2). (rac)-5-FBVM was obtained as a white powder in 25% yield.

4.3. Determination of optical rotation of (R,R)-5-FBVM and (S,S)-5-FBVM

The analytical separation of the 5-FBVM enantiomers by chiral HPLC was performed on a Reprosil Chiral-AM-RP column (250 × 4.6 mm), which is based on amylose-tris-(3,5-dimethylphenyl)-carbamate as chiral selector (Dr. Maisch-GmbH, Germany). The optical rotation was determined by using a chiral detector (OR 2090 model from JASCO, Germany). In general, the OR detector operated under following conditions: range: 0.05, response: SLOW, gain: 10. The polarity of signal amplitudes obtained by the chiral detector was checked with (–)-vesamicol as reference compound. By using 91% CH₃CN/20 mM NH₄OAc aq and a flow rate of 1 mL/min the enantiomers were separated. With *t*_R = 15.5 min the (–)-(R,R)-5-FBVM eluted in front of the (+)-(S,S)-5-FBVM with *t*_R = 23.5 min.

4.4. Receptor binding studies

For radioligand displacement studies, the test compounds were solved in DMSO at 10 mM stock solutions. Serial dilutions in the range of 0.01 nM to 1 μM were obtained by further dilution in incubation buffer.

VACHt affinity was determined by radioligand displacement studies on homogenates of PC12 cells stably transfected with rVACHt (Ali Roghani, Texas Tech University, Lubbock, TX, USA) by using (–)-[3H]vesamicol (Perkin Elmer; specific activity: 1296 GBq/mmol). Assays were incubated in 50 mM TRIS–HCl, pH

7.4 at room temperature. Incubation was terminated after 60 min by filtration (GF-B filter, pre-incubated in 0.3% PEI at room temperature for 90 min; Brandel Cell harvester). Non-specific binding was determined in the presence of 10 mM (±)-vesamicol.

σ₁ affinity was determined by radioligand displacement studies on homogenates of rat cortical membranes by using (–)-[3H]pentazocine (Perkin Elmer; specific activity: 1070 GBq/mmol). Assays were incubated in 50 mM TRIS–HCl, pH 7.4 at room temperature. Incubation was terminated after 120 min by filtration (GF-B filter, pre-incubated in 0.3% PEI at room temperature for 90 min; Brandel Cell harvester). Non-specific binding was determined in the presence of 10 μM haloperidol.

σ₂ affinity was determined by radioligand displacement studies on homogenates of rat liver membranes by using (–)-[3H]DTG (Perkin Elmer; specific activity: 1147 GBq/mmol) in the presence of 1 μM dextrallorphan (Roche) to block σ₁ binding of [3H]DTG. Assays were incubated in 50 mM TRIS–HCl, pH 7.4 at room temperature. Incubation was terminated after 120 min by filtration (GF-B filter, pre-incubated in 0.3% PEI at room temperature for 90 min; Brandel Cell harvester). Non-specific binding was determined in the presence of 10 μM haloperidol.

All assays were performed in triplicates at least three times. The IC₅₀-values were estimated by computational non-linear regression analysis. *K*_i-Values were calculated according to Cheng and Prusoff.⁵¹

Acknowledgment

This work was supported by INSERM. This study was funded in part by FEDER: ImAD project. We thank the 'Département d'analyses Chimiques et S.R.M. biologique et médicale' (Tours, France) for chemical analyses.

References and notes

- Bauer, J.; Hull, M.; Berger, M. Z. *Gerontol. Geriatr.* **1995**, *28*, 155.
- Terry, R. D.; Masliah, E.; Salmon, D. P.; Butters, N.; DeTeresa, R.; Hill, R.; Hansen, L. A.; Katzman, R. *Ann. Neurol.* **1991**, *30*, 572.
- Giboureau, N.; Emond, P.; Fulton, R. R.; Henderson, D. J.; Chalon, S.; Garreau, L.; Roselt, P.; Eberl, S.; Mavel, S.; Bodard, S.; Fulham, M. J.; Guilloteau, D.; Kassiou, M. *Synapse* **2007**, *61*, 962.
- Kilbourn, M. R.; Hockley, B.; Lee, L.; Sherman, P.; Quesada, C.; Frey, K. A.; Koeppe, R. A. *Nucl. Med. Biol.* **2009**, *36*, 489.
- Mulholland, G. K.; Jung, Y. W.; Wieland, D. M.; Kilbourn, M. R.; Kuhl, D. E. *J. Labelled Compd. Radiopharm.* **1993**, *33*, 583.
- Rogers, G. A.; Stone-Elander, S.; Ingvar, M.; Eriksson, L.; Parsons, S. M.; Widén, L. *Nucl. Med. Biol.* **1994**, *21*, 219.
- Efange, S. M.; Langason, R. B.; Khare, A. B.; Low, W. C. *Life Sci.* **1996**, *58*, 1367.
- Efange, S. M.; Khare, A.; Parsons, S. M.; Bau, R.; Metzenthin, T. *J. Med. Chem.* **1993**, *36*, 985.
- Sorger, D.; Scheunemann, M.; Vercouillie, J.; Grossmann, U.; Fischer, S.; Hiller, A.; Wenzel, B.; Roghani, A.; Schliebs, R.; Steinbach, J.; Brust, P.; Sabri, O. *Nucl. Med. Biol.* **2009**, *36*, 17.
- Sorger, D.; Scheunemann, M.; Großmann, U.; Fischer, S.; Vercouillie, J.; Hiller, A.; Wenzel, B.; Roghani, A.; Schliebs, R.; Brust, P.; Sabri, O.; Steinbach, J. *Nucl. Med. Biol.* **2008**, *35*, 185.
- Parsons, S. M.; Bahr, B. A.; Rogers, G. A.; Clarkson, E. D.; Noremborg, K.; Hicks, B. W. *Prog. Brain Res.* **1993**, *98*, 175.
- Bahr, B. A.; Clarkson, E. D.; Rogers, G. A.; Noremborg, K.; Parsons, S. M. *Biochemistry* **1992**, *31*, 5752.
- Altar, C. A.; Marien, M. R. *Synapse* **1988**, *2*, 486.
- Bahr, B. A.; Parsons, S. M. *Proc. Natl. Acad. Sci. U.S.A.* **1986**, *83*, 2267.
- Efange, S. M.; Mach, R. H.; Smith, C. R.; Khare, A. B.; Foulon, C.; Akella, S. K.; Childers, S. R.; Parsons, S. M. *Biochem. Pharmacol.* **1995**, *49*, 791.
- Ichikawa, T.; Ajiki, K.; Matsuura, J.; Misawa, H. *J. Chem. Neuroanat.* **1997**, *13*, 23.
- Phan, V. L.; Miyamoto, Y.; Nabeshima, T.; Maurice, T. *J. Neurosci. Res.* **2005**, *79*, 561.
- Jung, Y. W.; Van Dort, M. E.; Gildersleeve, D. L.; Wieland, D. M. *J. Med. Chem.* **1990**, *33*, 2065.
- Kuhl, D. E.; Minoshima, S.; Fessler, J. A.; Frey, K. A.; Foster, N. L.; Ficaró, E. P.; Wieland, D. M.; Koeppe, R. A. *Ann. Neurol.* **1996**, *40*, 399.
- Sorger, D.; Schliebs, R.; Kampfer, I.; Rossner, S.; Heinicke, J.; Dannenberg, C.; Georgi, P. *Nucl. Med. Biol.* **2000**, *27*, 23.

21. Zea-Ponce, Y.; Mavel, S.; Assaad, T.; Kruse, S. E.; Parsons, S. M.; Emond, P.; Chalon, S.; Giboureau, N.; Kassiou, M.; Guilloteau, D. *Bioorg. Med. Chem.* **2005**, *13*, 745.
22. Jung, Y. W.; Frey, K. A.; Mulholland, G. K.; del Rosario, R.; Sherman, P. S.; Raffel, D. M.; Van Dort, M. E.; Kuhl, D. E.; Gildersleeve, D. L.; Wieland, D. M. *J. Med. Chem.* **1996**, *39*, 3331.
23. Assaad, T.; Mavel, S.; Emond, P.; Chalon, S.; Drossard, M. L.; Vergote, J.; Bodard, S.; Allouchi, H.; Besnard, J.-C.; Guilloteau, D. *J. Labelled Compd. Radiopharm.* **2007**, *50*, 139.
24. Assaad, T.; Mavel, S.; Parsons, S. M.; Kruse, S.; Galineau, L.; Allouchi, H.; Kassiou, M.; Chalon, S.; Guilloteau, D.; Emond, P. *Bioorg. Med. Chem. Lett.* **2006**, *16*, 2654.
25. Emond, P.; Mavel, S.; Zea-Ponce, Y.; Kassiou, M.; Garreau, L.; Bodard, S.; Drossard, M. L.; Chalon, S.; Guilloteau, D. *Nucl. Med. Biol.* **2007**, *34*, 967.
26. Szymoszek, A.; Wenzel, B.; Scheunemann, M.; Steinbach, J.; Schüürmann, G. *J. Med. Chem.* **2008**, *51*, 2128.
27. Rogers, G. A.; Parsons, S. M.; Anderson, D. C.; Nilsson, L. M.; Bahr, B. A.; Kornreich, W. D.; Kaufman, R.; Jacobs, R. S.; Kirtman, B. *J. Med. Chem.* **1989**, *32*, 1217.
28. Rogers, D.; Hopfinger, A. J. *J. Chem. Inf. Comput. Sci.* **1994**, *34*, 854.
29. Stanton, D. T.; Jurs, P. C. *Anal. Chem.* **1990**, *62*, 2323.
30. Shiba, K.; Ogawa, K.; Ishiwata, K.; Yajima, K.; Mori, H. *Bioorg. Med. Chem.* **2006**, *14*, 2620.
31. Berkoff, C. E.; Rivard, D. E.; Kirkpatrick, D.; Ives, J. L. *Synth. Commun.* **1980**, *10*, 939.
32. Hashida, Y.; Landells, R. G. M.; Lewis, G. E.; Szele, I.; Zollinger, H. *J. Am. Chem. Soc.* **1978**, *100*, 2816.
33. Szele, I.; Zollinger, H. *J. Am. Chem. Soc.* **1978**, *100*, 2811.
34. Galli, C. *Chem. Rev.* **1988**, *88*, 765.
35. Garel, L.; Saint-Jalmes, L. *Tetrahedron Lett.* **2006**, *47*, 5705.
36. Doyle, M. P.; Bryker, W. J. *J. Org. Chem.* **1979**, *44*, 1572.
37. Laali, K. K.; Gettwert, V. J. *J. Fluorine Chem.* **2001**, *107*, 31.
38. Hubbard, A.; Okazaki, T.; Laali, K. K. *J. Org. Chem.* **2008**, *73*, 316.
39. Satyamurthy, N.; Barrio, J. R.; Schmidt, D. G.; Kammerer, C.; Bida, G. T.; Phelps, M. E. *J. Org. Chem.* **1990**, *55*, 4560.
40. Yoneda, N.; Fukuhara, T. *Tetrahedron* **1996**, *52*, 23.
41. Kimball, D. B.; Haley, M. M. *Angew. Chem., Int. Ed.* **2002**, *41*, 3338.
42. Berridge, M. S.; Sayre, L. M.; Arora, P. K.; Terris, A. H.; Riachi, N. J.; Harik, S. I. *J. Med. Chem.* **1993**, *36*, 1284.
43. Pages, T.; Langlois, B. R. *J. Fluorine Chem.* **2001**, *107*, 321.
44. Harmata, M.; Hong, X.; Zheng, P. *Tetrahedron Lett.* **2006**, *47*, 7343.
45. Schmidt, B. F.; Snyder, E. J.; Carroll, R. M.; Farnsworth, D. W.; Michejda, C. J.; Smith, R. H. *J. Org. Chem.* **1997**, *62*, 8660.
46. Smith, R. H.; Wladkowski, B. D.; Mehl, A. F.; Cleveland, M. J.; Rudrow, E. A.; Chmurny, G. N.; Michejda, C. J. *J. Org. Chem.* **1989**, *54*, 1036.
47. Tewson, T. J.; Welch, M. J. *J. Chem. Soc., Chem. Commun.* **1979**, 1149.
48. Barrio, J. R.; Satyamurthy, N.; Ku, H.; Phelps, M. E. *J. Chem. Soc., Chem. Commun.* **1983**, 443.
49. Pages, T.; Langlois, B. R.; Bars, D. L.; Landais, P. *J. Fluorine Chem.* **2001**, *107*, 329.
50. Rogers, G.; Kornreich, W.; Hand, K.; Parsons, S. *Mol. Pharmacol.* **1993**, *44*, 633.
51. Cheng, Y.; Prusoff, W. H. *Biochem. Pharmacol.* **1973**, *22*, 3099.
52. Shiba, K.; Yano, T.; Sato, W.; Mori, H.; Tonami, N. *Life Sci.* **2002**, *71*, 1591.
53. Efange, S. M. N.; von Hohenberg, K.; Khare, A. B.; Tu, Z.; Mach, R. H.; Parsons, S. *M. Nucl. Med. Biol.* **2000**, *27*, 749.